Local Linear Constraint based Optimization Model for Material Decomposition

Qian Wang[†], Yining Zhu[*‡§], Hengyong Yu[*†]
Email: Qian_Wang@student.uml.edu, ynzhu@cnu.edu.cn, hengyong-yu@ieee.org
[†]*Department of Electrical and Computer Engineering, University of Massachusetts Lowell, Lowell, Massachusetts, USA*
[‡]*School of Mathematical Sciences, Capital Normal University, Beijing, 100048, China*
[§]*Beijing Higher Institution Engineering Research Center of Testing and Imaging, Beijing, 100048, China*

***Abstract*—Dual spectral computed tomography (DSCT) has a superior material distinguishability than the conventional single spectral computed tomography (SSCT). However, the decomposition process is an illposed problem, which is sensitive to noise. Thus, the decomposed image quality is degraded, and the corresponding signal-to-noise ratio (SNR) is much lower than that of directly reconstructed image of SSCT. In this work, we establish a local linear relationship between the decomposed results of DSCT and SSCT. Based on this constraint, we propose an optimization model for DSCT and develop an iterative method with image guided filtering. Both numerical simulations and real experiments are performed to validate the effectiveness of the proposed approach.**

***Index Terms*—local linear constraint, optimization model, image guided filtering, dual spectral computed tomography.**

1. Introduction

In X-ray dual spectral computed tomography (DSCT), also known as dual energy computed tomography (DECT), a specimen is scanned with two different X-ray energy spectra. The collected polychromatic projections from this procedure are utilized to perform energy- and material-selective reconstructions [1], [2]. Compared with the conventional single spectral computed tomography (SSCT), DSCT has a superior material distinguishability. Therefore, it has wide applications in both medical and industrial domains [3], [4], [5], [6].

Existing methods to perform decomposition of DSCT can be classified into three groups: image based methods, projection based methods, and iterative methods. Image based methods treat the projection data sets of different spectra as being independent until the images are reconstructed. Images from all spectra are linearly combined to obtain two decomposed images [7]. Because such methods fail to describe the real nonlinearity relationship between decomposed results and polychromatic projections, the decomposition results will suffer from artifacts [3], [8]. Projection based methods treat the available information by passing the projection data through a high order decomposition function, followed by image reconstruction [9], [10]. Generally speaking, they can obtain better decomposition results than image based ones. However, the combination of polychromatic projections requires satisfying a geometrical consistency. Several iterative methods are proposed based on statistical models and nonlinear optimizations [11], [12], [13]. By introducing prior knowledge or establishing an approximate model, these methods improve the decomposed image quality effectively. However, their convergence rates are slow and the computational cost is high. Recently, an extended algebraic reconstruction technique (E-ART) for DSCT was proposed by Zhao et al. [14]. It describes the DSCT reconstruction as a nonlinear system problem, and extends the classic ART method to solve the model iteratively. While it can produce high quality decompositions, the convergence rate is slow, either. Hu et al. extended the E-ART method into an simultaneous version, i.e. E-SART [15]. This method is based on the matrix inversion and has a high degree of parallelism. Thus, the convergence speed of its parallel implementation is improved dramatically. But, the illposedness of the decomposition process renders it noticeably sensitive to noise, resulting in reduced signal-to-noise ratio (SNR).

Although SSCT has weaker capability for material distinguishing, the achieved SNR is dramatically higher than that of DSCT. Moreover, there is an interesting relationship, i.e., decomposed results of DSCT can be viewed as modifications of reconstructed images of SSCT by removing some components and adjusting gray values. Further, this structure-based feature can be mathematically described as a local linear relationship. By incorporating this constraint into an optimization model, the reconstructed image of SSCT could work as a reference to effectively improve the smoothness of decomposed results of DSCT. Thus, the systematic noise is well suppressed and the quality of decomposed results is considerably improved.

The remainder of this paper is organized as follows. In section 2, the mathematical model of DSCT is presented, and the E-SART method and the image guided filtering technique are briefly reviewed. In section 3, we present the local linear constraint based optimization model for DSCT and develop an iterative method with image guided filtering. In section 4, both numerical simulations and real experiments are performed to verify the effectiveness of the proposed methods. In last section, we discuss some related

. * Corresponding author.

issues and conclude this paper.

2. Theorical Methods

2.1. Mathematical Model of DSCT

By considering the fact that X-ray spectrum is polychromatic and assuming that collected raw data are geometrically consistent, we describe the physical process of DSCT as follows,

$$P_{k,l} = -\ln \int_E S_k(E) \exp\big(-\mathcal{P}_l(\mu(E,\mathbf{x}))\big)\,\mathrm{d}E, l \in \mathcal{L}, k = 1,2, \quad (1)$$

where $\mu(E,\mathbf{x})$ is the linear attenuation coefficient of a specimen at a spatial position $\mathbf{x}$ and energy E, $\mathcal{P}_l(\cdot)$ represents the ray transform which is an integral transform along a ray path l, $S_k(E)$ is the k-th normalized emission spectrum, $P_{k,l}$ indicates the acquired information frequently named projection data.

In DSCT, $\mu(E,\mathbf{x})$ is usually considered splittable with respect to variables E and $\mathbf{x}$,

$$\mu(E,\mathbf{x}) = \sum_{i=1}^{2} \psi_i(E) f_i(\mathbf{x}), \quad (2)$$

where $\psi_i(E)$ is a function of energy and $f_i(\mathbf{x})$ is a function of position. There are commonly two physical explanations for eq. (2): basis material based decomposition and effect based decomposition. For the former, $\psi_i(E)$ is the mass attenuation coefficient for material i, and $f_i(\mathbf{x})$ is the correlative density distribution. For the latter, $\psi_1(E) = E^{-3}$ and $\psi_2(E) = KN(E)$ (Klein-Nishina function) corresponds to the photoelectric effect and Compton scattering respectively, and $f_i(\mathbf{x})$ represents the correspondingly effect distribution. The aim of DSCT is to reconstruct images of distribution functions $f_i(\mathbf{x}), i = 1,2$.

2.2. E-SART Method

By substituting eq. (2) into eq. (1) and discretizing the correlative result, we get

$$P_{k,l} = -\ln\Big(\sum_{j=1}^{J_k} S_{k,j} \exp\big(-\sum_{i=1}^{2} \psi_{i,j}\mathcal{P}_l(\mathbf{f}_i)\big)\Delta E\Big), \quad (3)$$

where J_k is the energy bin number of spectrum k, ΔE represents the bin length, $S_{k,j}$ and $\psi_{i,j}$ are the samplings of $S_k(E)$ and $\psi_i(E)$ within bin j, and $\mathbf{f}_i$ is a one dimensional column vector representing the discretized distribution function. The 1st order Taylor expansion of eq. (3) at point $(\mathbf{f}_1(n);\mathbf{f}_2(n))$ is

$$P_{k,l} \approx P_{k,l}(n) + \Big(\tfrac{\Psi^1_{k,l}(n)}{Q_{k,l}(n)}, \tfrac{\Psi^2_{k,l}(n)}{Q_{k,l}(n)}\Big) \begin{pmatrix}\mathcal{P}(\mathbf{f}_1 - \mathbf{f}_1(n))\\ \mathcal{P}(\mathbf{f}_2 - \mathbf{f}_2(n))\end{pmatrix}, \quad (4)$$

where n indecates the current iteration step and

$$P_{k,l}(n) = -\ln\sum_{j=1}^{J_k} S_{k,j}\exp\big(-\sum_{i=1}^{2}\psi_{i,j}\mathcal{P}_l(\mathbf{f}_i(n))\big)\Delta E,$$
$$Q_{k,l}(n) = \sum_{j=1}^{J_k} S_{k,j}\exp\big(-\sum_{i=1}^{2}\psi_{i,j}\mathcal{P}_l(\mathbf{f}_i(n))\big)\Delta E,$$
$$\Psi^1_{k,l}(n) = \sum_{j=1}^{J_k} \psi_{1,j}S_{k,j}\exp\big(-\sum_{i=1}^{2}\psi_{i,j}\mathcal{P}_l(\mathbf{f}_i(n))\big)\Delta E,$$
$$\Psi^2_{k,l}(n) = \sum_{j=1}^{J_k} \psi_{2,j}S_{k,j}\exp\big(-\sum_{i=1}^{2}\psi_{i,j}\mathcal{P}_l(\mathbf{f}_i(n))\big)\Delta E.$$

Along each ray path, two projections are acquired based on different X-ray spectra. By solving the system of linear equation (4), for $k = 1,2$, we can get the projection of distribution function in an iteration form,

$$\begin{pmatrix}\mathcal{P}(\mathbf{f}_1(n+1))\\ \mathcal{P}(\mathbf{f}_2(n+1))\end{pmatrix} = \begin{pmatrix}\mathcal{P}(\mathbf{f}_1(n))\\ \mathcal{P}(\mathbf{f}_2(n))\end{pmatrix} + \frac{C_l(n)}{\det(M_l(n))}\begin{pmatrix}P_{1,l} - P_{1,l}(n)\\ P_{2,l} - P_{2,l}(n)\end{pmatrix},$$

where

$$M_l(n) = \begin{pmatrix}\frac{\Psi^1_{1,l}(n)}{Q_{1,l}(n)}, \frac{\Psi^2_{1,l}(n)}{Q_{1,l}(n)}\\ \frac{\Psi^1_{2,l}(n)}{Q_{2,l}(n)}, \frac{\Psi^2_{2,l}(n)}{Q_{2,l}(n)}\end{pmatrix}, C_l(n) = \begin{pmatrix}\frac{\Psi^2_{2,l}(n)}{Q_{2,l}(n)}, -\frac{\Psi^2_{1,l}(n)}{Q_{1,l}(n)}\\ -\frac{\Psi^1_{2,l}(n)}{Q_{2,l}(n)}, \frac{\Psi^1_{1,l}(n)}{Q_{1,l}(n)}\end{pmatrix}.$$

By using the conventional Simultaneous Algebraic Reconstruction Technique (SART), distribution function $\mathbf{f}_1$ and $\mathbf{f}_2$ are updated iteratively.

Comparing with E-ART, the parallel implementation of E-SART improves the convergence speed dramatically. However, the illposedness of the inverse problem renders this matrix inversion based decomposition process sensitive to inevitable systematic noise. Thus, some prior knowledge or constraints are needed to improve the robust against noise.

2.3. Image Guided Filtering

Guided filter [16], [17] is edge-preserving with a great variety of applications, of which the key assumption is a local linear model between a reference image I and the filtering output y,

$$y_i = a_k I_i + b_k, \forall i \in \omega_k, \quad (5)$$

where ω_k is a window centered at the pixel k, (a_k, b_k) are some linear coefficients constant in ω_k. Modeling the output y as the input x removing some unwanted noise or textures t:

$$y_i = x_i - t_i.$$

Thus, by minimizing the difference between y and x within a window ω_k while maintaining the linear model (5), the correlative optimization model is established as follow,

$$\min_{(a_k,b_k)} \sum_{i\in\omega_k} \big((a_k I_i + b_k - x_i)^2 + \epsilon a_k^2\big),$$

where ϵ is a regularization parameter penalizing large a_k. The solution given by [17] reads,

$$a_k = \frac{\frac{1}{|\omega|}\sum_{i\in\omega_k} I_i x_i - \nu_k \bar{x}_k}{\sigma_k^2 + \epsilon},$$
$$b_k = \bar{x}_k - a_k \nu_k,$$

where ν_k and σ_k^2 are the mean and variance of I in ω_k, $|\omega|$ is the number of pixels in ω_k, and $\bar{x}_k$ is the mean of x in ω_k. The filtering output y can be computed by employing eq. (5). Because a pixel i is involved in all the covered windows, by averaging all the possible output values, we get

$$y_i = \bar{a}_i I_i + \bar{b}_i.$$

Here $\bar{a}_i$ and $\bar{b}_i$ are the average coefficients of all windows covering pixel i. By using the image guided filtering, input x is refined by the reference image I based on the local linear relationship between them.

3. Algorithm Development

3.1. Local Linear Constraint based Optimization Model

Although the directly reconstructed images of SSCT have a weak capability to distinguish materials, the quality is significantly better than the decomposed results of DSCT, especially when the noise level is relatively high. Moreover, there are structure-based relationships between them. An intuitionistic character is that decomposed results of DSCT can be viewed as modifications of reconstructed images of SSCT by removing some components and adjusting gray values. When analyzing this feature in detail, as is illustrated in Fig. 1, we find that a linear relationship usually hold in small patches, and its discrete version reads,

$$\mathbf{f}^{(j)} = a^{(k)}\mathbf{g}^{(j)} + b^{(k)}, \forall j \in \omega^{(k)},$$

where $\mathbf{f}$ represents a decomposed result of DSCT, $\mathbf{g}$ represents a reconstructed image of SSCT, and j and k are pixel indexes.

Based on this constraint, we proposed an optimization model for DSCT as follows,

$$\min_{(\mathbf{f}_1,\mathbf{f}_2)} \left\{ \left\| \begin{pmatrix} \mathcal{P}(\mathbf{f}_1) - \mathcal{P}(\mathbf{f}_1(n)) \\ \mathcal{P}(\mathbf{f}_2) - \mathcal{P}(\mathbf{f}_2(n)) \end{pmatrix} - \frac{C_l(n)}{\det(M_l(n))} \begin{pmatrix} P_{1,l} - P_{1,l}(n) \\ P_{2,l} - P_{2,l}(n) \end{pmatrix} \right\|_{L_2}^2 + \sum_{i=1}^{2} \sum_k \sum_{j\in\omega_i^{(k)}} \frac{\xi_i}{|\omega_i|} \left((a_i^{(k)}\mathbf{g}_{\mathbf{f}_i}^{(j)} + b_i^{(k)} - \mathbf{f}_i^{(j)}(n))^2 + \epsilon_i (a_i^{(k)})^2 \right) \right\}, \quad (6)$$

where $\mathbf{g}_{\mathbf{f}_i}$ is a selected result of SSCT corresponding to $\mathbf{f}_i$, ξ_i and ϵ_i are regularization parameters.

In model (6), for each searched-for decomposed result, we employ a correlative local linear constraint. Thus, the smoothness knowledge from SSCT is effectively introduced into the decomposition process. By weakening the illposedness, the noise is noticeably suppressed, and SNR is dramatically improved.

3.2. Iterative Reconstruction Algorithm

Considering the facts that the data term is measured in projection domain and the regularity terms are measured in image domain, we split model (6) into two sub-optimization problems and develop an iterative scheme as follows,

$$(\mathcal{P}(\mathbf{f}_1(*)), \mathcal{P}(\mathbf{f}_2(*))) = \min_{(\mathcal{P}(\mathbf{f}_1),\mathcal{P}(\mathbf{f}_2))} \left\| \begin{pmatrix} \mathcal{P}(\mathbf{f}_1) - \mathcal{P}(\mathbf{f}_1(n)) \\ \mathcal{P}(\mathbf{f}_2) - \mathcal{P}(\mathbf{f}_2(n)) \end{pmatrix} - \frac{C_l(n)}{\det(M_l(n))} \begin{pmatrix} P_{1,l} - P_{1,l}(n) \\ P_{2,l} - P_{2,l}(n) \end{pmatrix} \right\|_{L_2}^2, \quad (7a)$$

$$(\mathbf{f}_1(*), \mathbf{f}_2(*)) = \mathcal{P}^{-1}(\mathcal{P}(\mathbf{f}_1(*)), \mathcal{P}(\mathbf{f}_2(*))), \quad (7b)$$

$$(a_i(n+1)), b_i(n+1))) = \min_{(a_i,b_i)} \sum_k \sum_{j\in\omega_i^{(k)}} \frac{\xi_i}{|\omega_i|} \left((a_i^{(k)}\mathbf{g}_{\mathbf{f}_i}^{(j)} + b_i^{(k)} - \mathbf{f}_i^{(j)}(*))^2 + \epsilon_i (a_i^{(k)})^2 \right), \quad (7c)$$

$$\bar{a}_i^{(k)}(n+1) = \frac{1}{|\omega_i|} \sum_{j\in\omega_i^{(k)}} a_i^{(j)}(n+1), \quad (7d)$$

$$\bar{b}_i^{(k)}(n+1) = \frac{1}{|\omega_i|} \sum_{j\in\omega_i^{(k)}} b_i^{(j)}(n+1), \quad (7e)$$

$$\mathbf{f}_i(n+1) = \bar{a}_i(n+1)\mathbf{g}_{\mathbf{f}_i} + \bar{b}_i(n+1), \quad (7f)$$

where $\bar{a}_i(n+1)$ and $\bar{b}_i(n+1)$ are the averaged $a_i(n+1)$ and $b_i(n+1)$ within the window ω_i, eqs. (7c)-(7f) are implemented for $i = 1, 2$, respectively. We use the E-SART method for eqs. (7a) and (7b), and the image guided filtering for eqs. (7c)-(7f).

4. Experimental Results

To verify the effectiveness of the proposed method, experiments are performed with both simulated and real data sets. In the numerical simulations, both noise-free and noisy cases are tested. Fan beam geometry is assumed for all the experiments for simplicity. As a comparison, we implemented the E-SART method as well. We employ all the methods for the case of basis material based decomposition, which can be easily extended to the effect based case.

4.1. Numerical Simulations

The phantom is 2D FORBILD head phantom without ears shown in Fig. 1 [18]. Water and bone are chosen as two basis materials, and the corresponding mass attenuation coefficients are retrieved from the National Institute of Standard Technology (NIST) tables [19]. A polychromatic spectrum of a GE Maxiray 125 X-ray tube is simulated by using an open source X-ray spectra simulator, SpectrumGUI [20]. Two tube voltages, 80 kV and 140 kV, are chosen, where the latter is filtered with 1.0 mm copper. The correlative spectra are shown in Fig. 2. The energy of photons emitted from the source is 8 MeV. The detector consists of 512 channels with length 0.3 mm. The source-object distance (SOD) is 1000 mm and the source-detector distance (SDD) is 1200 mm. With this configuration, 512×512 images are reconstructed with a pixel size of 0.249×0.249 mm^2.

Under this setting, we test the noise-free case and the noisy case by using the E-SART and the proposed method, respectively (see Figs. 3 and 4). Moreover, three common

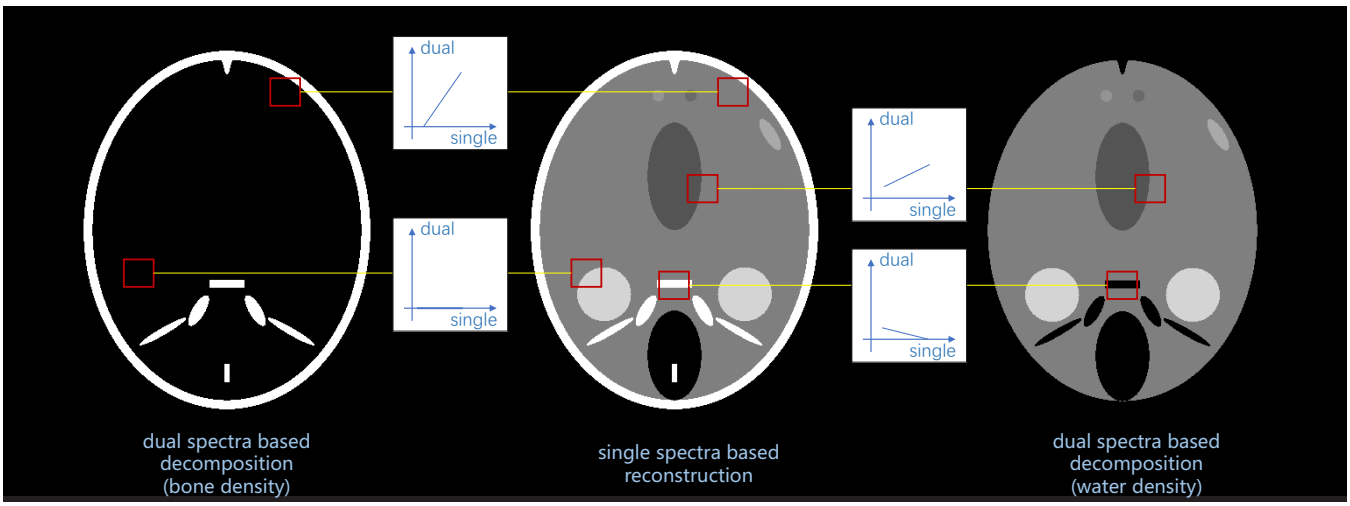

Figure 1. Illustration of the local linear relationship. Image directly reconstructed from single spectra is shown in the middle column, dual spectra based decomposed results are shown in the left (bone density) and the right (water density) columns.

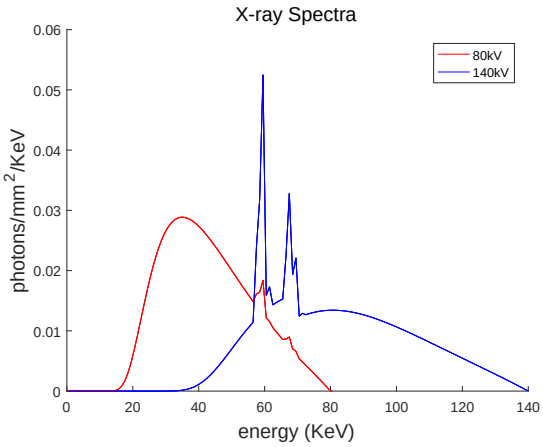

Figure 2. The X-ray spectra used in the numerical simulations.

image quality evaluations are employed, i.e., peak signal-to-noise ratio (PSNR), normal mean absolute deviation (NMAD) and structural similarity (SSIM). The corresponding results are shown in Tables 1 and 2. For both methods, the iteration number is fixed to 6. All the experimental results demonstrate the merits of noise tolerance for the proposed method.

TABLE 1. PSNR, NMAD AND SSIM OF NUMERICAL SIMULATION RESULTS FROM NOISE-FREE PROJECTIONS.

		PSNR	NMAD	SSIM
Bone density	E-SART Method	17.8298	0.516727	0.928197
	Proposed Method	18.3021	0.507613	0.941834
Water density	E-SART Method	13.2118	0.424380	0.670655
	Proposed Method	15.9604	0.309683	0.799645
70 KeV μ-image	E-SART Method	22.1476	0.147212	0.684622
	Proposed Method	26.2219	0.064983	0.822715

TABLE 2. PSNR, NMAD AND SSIM OF NUMERICAL SIMULATION RESULTS FROM NOISY PROJECTIONS.

		PSNR	NMAD	SSIM
Bone density	E-SART Method	17.5202	0.530706	0.921841
	Proposed Method	17.8209	0.523427	0.93074
Water density	E-SART Method	13.2000	0.422779	0.665225
	Proposed Method	15.9502	0.311418	0.850024
70 KeV μ-image	E-SART Method	21.8233	0.155406	0.673225
	Proposed Method	26.4040	0.051748	0.875444

4.2. Real Experiments

In the real experiment, the measured specimen is a bone submerged in water. An X-ray source (YXLON Y.TU450 D09 tube) is operated at the tube voltage of 80 kV and 140 kV for low- and high-energy spectra scan, respectively. The tube current is 5 mA. The employed flat-panel detector (YXLON Y.LDA detector) has 1920×1920 detector cells with mesh size of 0.127 mm. The SOD is 231.5 mm and the SDD is 696.7 mm. By using a collimator, the data from the central slice are obtained to validate the proposed method. The iteration number is 10.

The decomposed results by using the E-SART method and the proposed method are shown in Fig. 5. It is noticeable that the proposed method can effectively suppress the noise and dramatically improve the smoothness.

5. Discussion and Conclusion

In this work, we establish a local linear constraint to describe the structure relationship between dual spectra based decomposed results and single spectrum based reconstruction. A correlative optimization model and an iterative algorithm are proposed, respectively. By employing

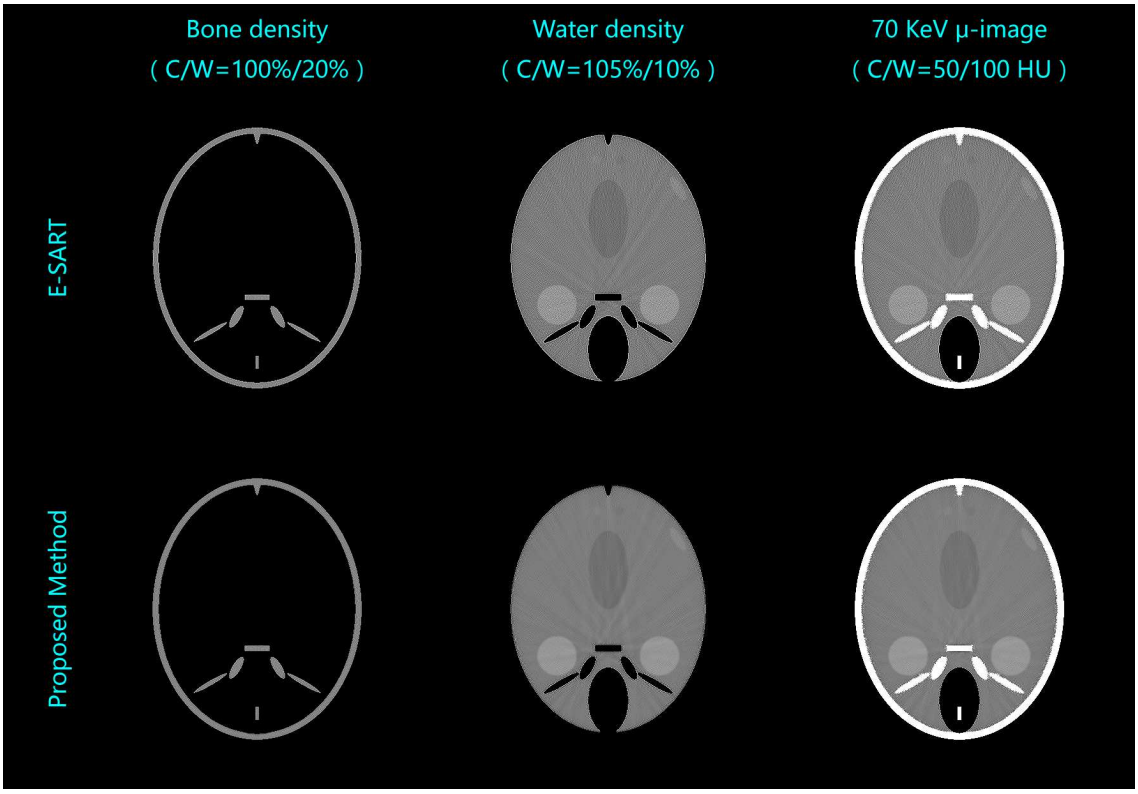

Figure 3. Numerical simulation results from noise-free projections.

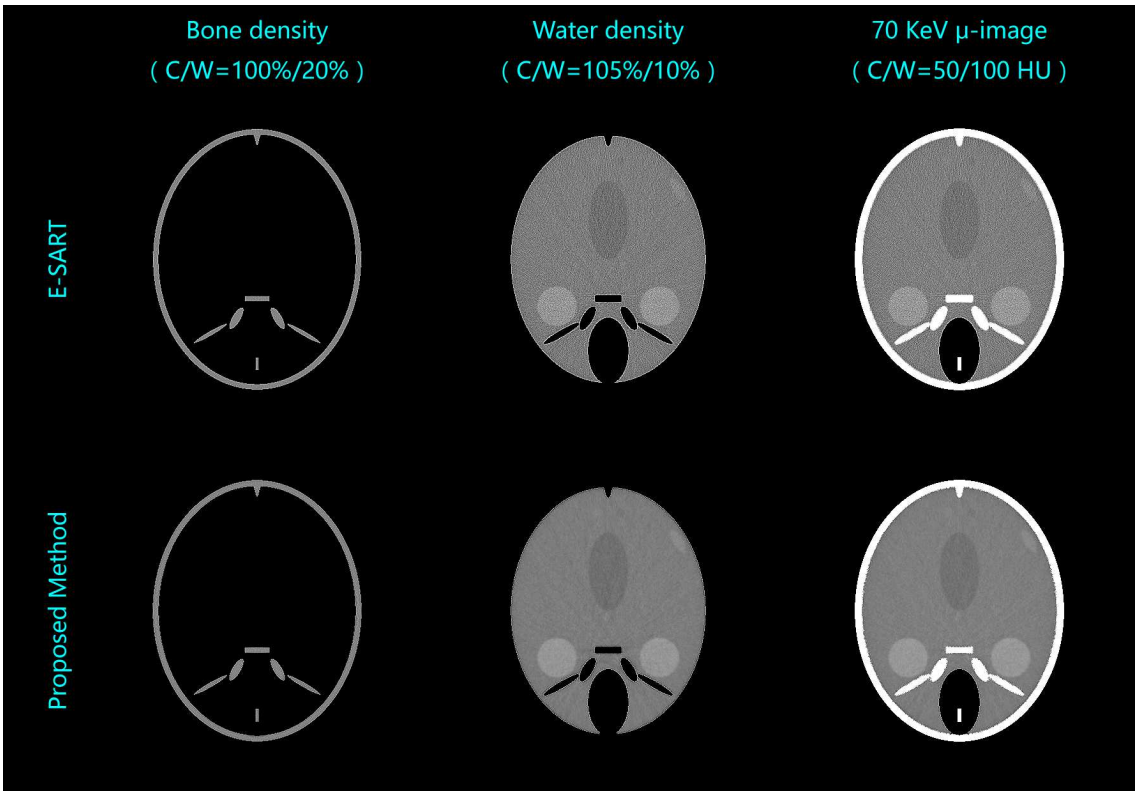

Figure 4. Numerical simulation results from noisy projections.

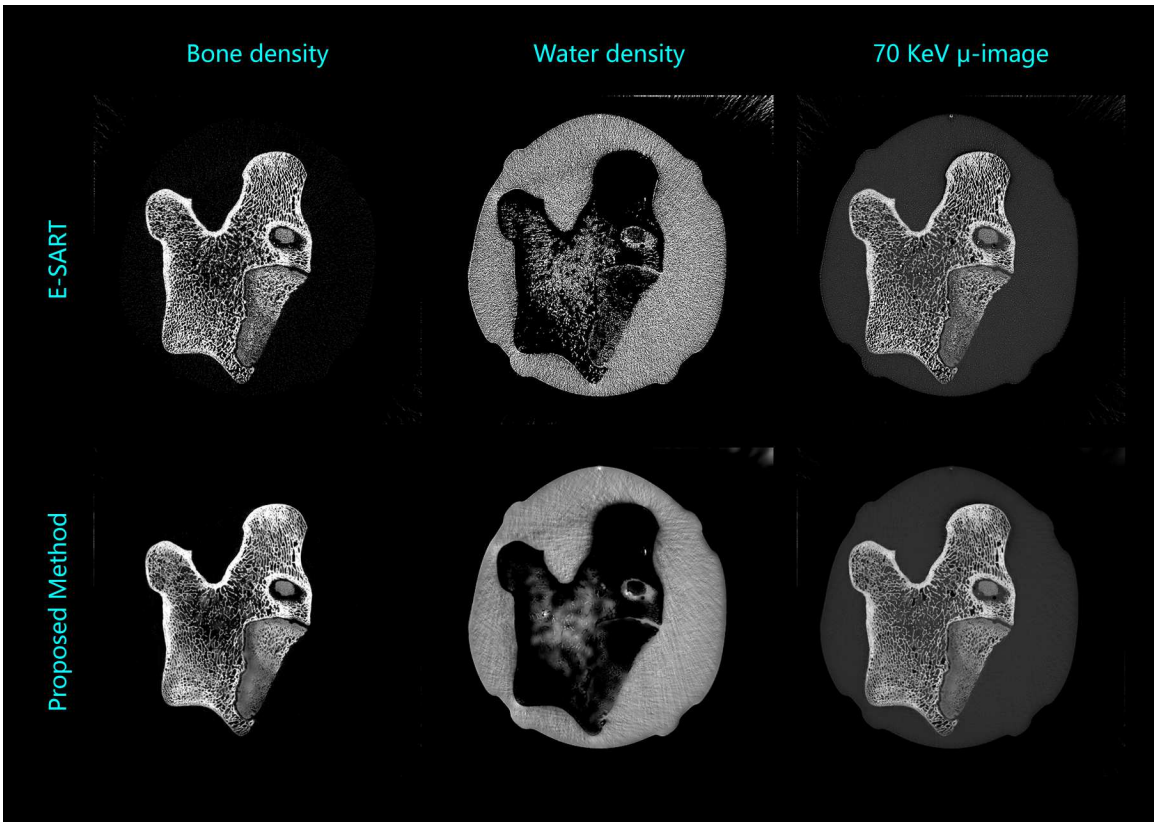

Figure 5. Real experiments by using the E-SART method (the first row) and the proposed method (the second row).

the image guided filtering, the smoothness knowledge of the single spectrum based image is effectively introduced into the decomposition process. Because this method reduces the illposedness of the DSCT, the noise in the decomposition process is significantly suppressed. Both numerical simulations and real experiments demonstrate the merits of the proposed method.

On one hand, the proposed method suppresses the noise effectively, and the quality of decomposed results is dramatically improved. On the other hand, it maintains the merits of fast convergence rate of the E-SART. Further quantitative analyses and comparisons are needed to choose a satisfactory reference image, which will be fully studied in our future work.

Acknowledgments

This work was supported in part by NIH/NIBIB U01 grant EB017140. It was also supported by the National Natural Science Foundation of China grant 61501310 and 61372179, and by the Beijing Municipal Commission of Education grant KM201710028002.

References

[1] R. E. Alvarez and A. Macovski, "Energy-selective reconstructions in x-ray computerised tomography," *Physics in medicine and biology*, vol. 21, no. 5, p. 733, 1976.

[2] R. Alvarez and E. Seppi, "A comparison of noise and dose in conventional and energy selective computed tomography," *IEEE Transactions on Nuclear Science*, vol. 26, no. 2, pp. 2853–2856, 1979.

[3] A. J. Coleman and M. Sinclair, "A beam-hardening correction using dual-energy computed tomography," *Physics in medicine and biology*, vol. 30, no. 11, p. 1251, 1985.

[4] P. E. Kinahan, A. M. Alessio, and J. A. Fessler, "Dual energy CT attenuation correction methods for quantitative assessment of response to cancer therapy with PET/CT imaging," *Technology in cancer research & treatment*, vol. 5, no. 4, pp. 319–327, 2006.

[5] Z. Ying, R. Naidu, and C. R. Crawford, "Dual energy computed tomography for explosive detection," *Journal of X-ray Science and Technology*, vol. 14, no. 4, pp. 235–256, 2006.

[6] T. Johnson, C. Fink, S. O. Schönberg, and M. F. Reiser, *Dual energy CT in clinical practice*. Springer Science & Business Media, 2011.

[7] C. Maaß, M. Baer, and M. Kachelrieß, "Image-based dual energy CT using optimized precorrection functions: A practical new approach of material decomposition in image domain," *Medical physics*, vol. 36, no. 8, pp. 3818–3829, 2009.

[8] R. A. Brooks and G. Di Chiro, "Beam hardening in x-ray reconstructive tomography," *Physics in medicine and biology*, vol. 21, no. 3, p. 390, 1976.

[9] T. G. Flohr, C. H. McCollough, H. Bruder, M. Petersilka, K. Gruber, C. Süβ, M. Grasruck, K. Stierstorfer, B. Krauss, R. Raupach *et al.*, "First performance evaluation of a dual-source CT (DSCT) system," *European radiology*, vol. 16, no. 2, pp. 256–268, 2006.

[10] P. Stenner, T. Berkus, and M. Kachelriess, "Empirical dual energy calibration (EDEC) for cone-beam computed tomography," *Medical physics*, vol. 34, no. 9, pp. 3630–3641, 2007.

[11] I. A. Elbakri and J. A. Fessler, "Statistical image reconstruction for polyenergetic X-ray computed tomography," *IEEE transactions on medical imaging*, vol. 21, no. 2, pp. 89–99, 2002.

[12] C. Maaß, R. Grimmer, and M. Kachelrieß, "Dual energy CT material decomposition from inconsistent rays (MDIR)," in *2009 IEEE Nuclear Science Symposium Conference Record (NSS/MIC)*. IEEE, 2009, pp. 3446–3452.

[13] T. Niu, X. Dong, M. Petrongolo, and L. Zhu, "Iterative image-domain decomposition for dual-energy CT," *Medical physics*, vol. 41, no. 4, p. 041901, 2014.

[14] Y. Zhao, X. Zhao, and P. Zhang, "An extended algebraic reconstruction technique (E-ART) for dual spectral CT," *IEEE transactions on medical imaging*, vol. 34, no. 3, pp. 761–768, 2015.

[15] J. Hu, X. Zhao, and F. Wang, "An extended simultaneous algebraic reconstruction technique (E-SART) for X-ray dual spectral computed tomography," *Scanning*, 2016.

[16] K. He, J. Sun, and X. Tang, "Guided image filtering," in *European conference on computer vision*. Springer, 2010, pp. 1–14.

[17] ——, "Guided image filtering," *IEEE transactions on pattern analysis and machine intelligence*, vol. 35, no. 6, pp. 1397–1409, 2013.

[18] G. Lauritsch and H. Bruder, "FORBILD head phantom," website: http://www.imp.uni-erlangen.de/forbild/deutsch/results/head/head.html.

[19] J. H. Hubbell and S. M. Seltzer, "Tables of x-ray mass attenuation coefficients and mass energy-absorption coefficients 1 kev to 20 mev for elements z= 1 to 92 and 48 additional substances of dosimetric interest," National Inst. of Standards and Technology-PL, Gaithersburg, MD (United States). Ionizing Radiation Div., Tech. Rep., 1995.

[20] "Spectrumgui," website: https://sourceforge.net/projects/spectrumgui/.